Modeling for characterizing defects in plates using two-dimensional maps of instantaneous ultrasonic out-of-plane displacement obtained by pulsed TV-Holography

J. Carlos López-Vázquez[a,*], J. Luis Deán[a], Cristina Trillo[a], Ángel F. Doval[a], José L. Fernández[a], Faisal Amlani[b] and Oscar P. Bruno[b]

[a]Departamento de Física Aplicada. Universidade de Vigo. E. T. S. de Enxeñeiros Industriais. Campus Universitario. 36310 Vigo (Spain).
[b]Applied and Computational Mathematics, California Institute of Technology 217-50, Pasadena, California 91125 (USA).

ABSTRACT

It has been demonstrated that non-destructive inspection of plates can be performed by using two-dimensional maps of instantaneous out-of-plane displacements obtained with a self-developed pulsed TV-holography system. Specifically, the interaction of guided elastic waves with defects produces scattering patterns that contain information about the defects (position, dimensions, orientation, etc.). For quantitative characterization on this basis, modeling of the wave propagation and interaction with the defects is necessary. In fact, the development of models for scattering of waves in plates is yet an active research field in which the most reliable approach is usually based on the rigorous formulation of elasticity theory. By contrast, in this work the capability of a simple two-dimensional scalar model for obtaining a quantitative description of the output two-dimensional maps associated to artificial defects in plates is studied. Some experiments recording the interaction of narrowband Rayleigh waves with artificial defects in aluminum plates are presented, in which the acoustic field is obtained from the TV-holography optical phase-change maps by means of a specially developed two-step spatio-temporal Fourier transform method. For the modeling, harmonic regime and free-stress boundary conditions are assumed. Comparisons between experimental and simulated maps are included for defects with different shapes.

Keywords: Pulsed TV holography, ESPI, Guided waves, Elastic scattering

1. INTRODUCTION

Ultrasonic techniques are routinely employed for non-destructive testing (NDT) and evaluation of plate-like structures in industry.[1] Along the last three decades many new developments have been introduced that have provided assessment results progressively more quantitative in an increasing number of applications. This has been possible due to the simultaneous advances in theoretical studies of elastic wave propagation and scattering and developments of numerical techniques that provide approximate solutions in practical applications.[2]

In our case, we have demonstrated that non-destructive inspection of plates can be performed by using two-dimensional acoustic fields of instantaneous out-of-plane displacements obtained with a self-developed pulsed TV-holography system.[3,4] The ultrasonic two-dimensional field maps the elastic wave scattering patterns, that contain information related to defects (position, dimensions, orientation, etc.). For obtaining a quantitative characterization on this basis, the most direct and reliable possibility would be to adapt to our system output one of the existing numerical schemes based on the vectorial linear theory of elasticity (f.i. references 5–9). Nevertheless, selection among this wide spectrum of possible models (and its subsequent adaptation) is far from being direct in our case and the main reasons are twofold. On the one hand, in contrast to more classical ultrasonic schemes (pulse-echo or pitch-catch classical configurations) that provide outputs with high temporal resolution and low spatial information content, our system presents complementary characteristics providing information with high spatial resolution, i.e. a large number of spatial samples (about 10^6), at a much smaller number of

*E-mail: jclopez@uvigo.es

Optical Measurement Systems for Industrial Inspection VI, edited by Peter H. Lehmann, Proc. of SPIE Vol. 7389, 738937 · © 2009 SPIE · CCC code: 0277-786X/09/$18 · doi: 10.1117/12.827819

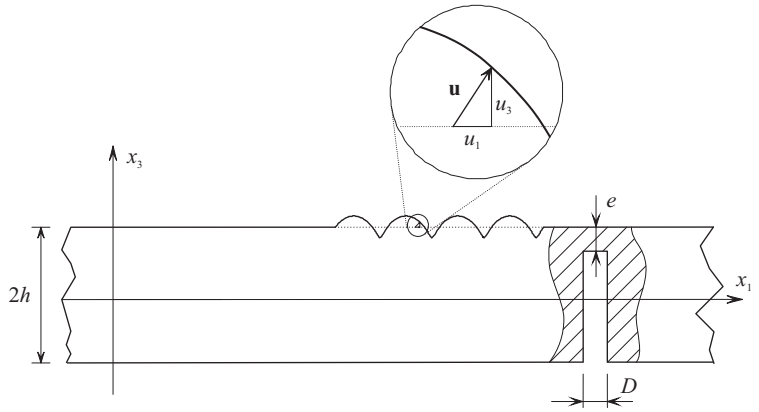

Figure 1. Scheme of a plate of thickness $2h$ with a cylindrical defect of diameter D and residual depth e.

temporal samples (typically 8). On the other hand, the field of view of the detected two-dimensional scattering pattern contains tens of ultrasonic wavelengths, which means that the modeling of the wave propagation and interaction has to be adequate within the mid-high frequency range. These two features invalidate or limit the applicability of many existing approaches that have been designed for high temporal resolution outputs and/or low frequency regime.

An alternative to vectorial models is to employ simplified theories as the basis for numerical or analytical approximations. These type of models, that are valid only for a limited number of situations but that occur often in practice, could have a wide applicability. In this context, plate theories have been employed recently for analyzing the scattering of guided waves by cylindrical inclusions in plates.[10] Also, a two-dimensional scalar model has been employed for solving the inverse problem of scattering by cylindrical inclusions in plates using experimental data obtained with a TV-holography technique close to ours.[11] Reported results in reference 11 also include the presentation of simulated scattering patterns for different defect types but a direct comparison between simulated and experimental ultrasonic field values is not presented.

In this work we study the capability of this two-dimensional scalar model for obtaining a quantitative description of the output two-dimensional maps associated to artificial defects in plates. We introduce the theoretical framework for modeling in the harmonic regimen. Then we describe the TV-holography experimental system for elastic wave detection and the procedure for obtaining the 2D acoustic field from optical phase-change maps by means of a specially developed Fourier transform method. Also it is stated a brief outline of the state-of-the art numerical method employed for obtaining simulated scattering data. Interactions of narrowband guided waves with artificial defects in aluminum plates are recorded and compared with the corresponding simulated patterns. To the best of our knowledge this is the first time that such a comparison is presented.

2. THEORETICAL FRAMEWORK

2.1 Linear elasticity theory

Basic relation of linear elasticity theory[12] are included here to establish notation and the framework of the simplified scalar model presented later in section 2.3. Referring to the geometry of figure 1 (x_1, x_2, x_3) denote cartesian coordinates, $\mathbf{u} = (u_1, u_2, u_3)$ the displacement vector and

$$\epsilon_{ij} = \frac{1}{2}\left(\frac{\partial u_i}{\partial x_j} + \frac{\partial u_j}{\partial x_i}\right) \tag{1}$$

are the components of the strain tensor $\boldsymbol{\epsilon}$ for the small (infinitesimal) strain regimen. In the case of a linear isotropic solid its material characteristics can be specified only by Lamé constants λ_{L} and μ_{L} and the stress-strain relationship simplifies to

$$\tau_{ij} = \lambda_{\mathrm{L}}\delta_{ij}\sum_k \epsilon_{kk} + 2\mu_{\mathrm{L}}\epsilon_{ij} \tag{2}$$

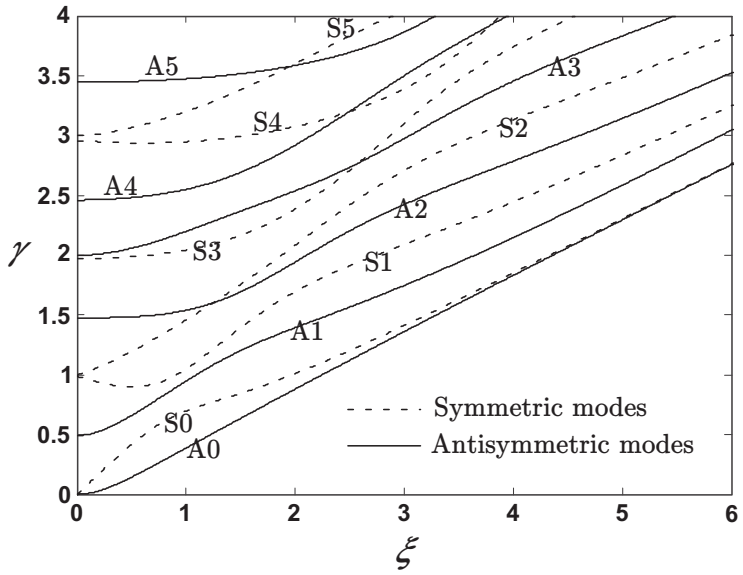

Figure 2. Frequency spectrum of Lamb modes for a plate with stress-free boundaries, $\gamma = 2h\omega/\pi c_{\mathrm{L}}$ and $\xi = 2hk_1/\pi$ are the normalized frequency and wavenumber respectively

being δ_{ij} the Kronecker delta. In the following we restrict ourselves to harmonic time dependence in such a way that for a single temporal frequency f we have

$$\mathbf{u}\left(\mathbf{r},t\right) = \mathrm{Re}\left[\hat{\mathbf{u}}\left(\mathbf{r},t\right)\right] = \mathrm{Re}\left[\hat{\mathbf{u}}_{\mathrm{m}}\left(\mathbf{r}\right)\exp\left(j2\pi ft\right)\right] \tag{3}$$

being $\hat{\mathbf{u}}$ the complex displacement, $\hat{\mathbf{u}}_{\mathrm{m}}$ the complex amplitude vector of the wave and j the imaginary unit. In this conditions, employing (1) and (2) in balance momentum equation for a region free of body forces results

$$\left(\lambda_{\mathrm{L}} + \mu_{\mathrm{L}}\right)\nabla\left(\nabla\cdot\hat{\mathbf{u}}_{\mathbf{m}}\right) + \mu_{\mathrm{L}}\nabla^2\hat{\mathbf{u}}_{\mathbf{m}} + \rho\omega^2\hat{\mathbf{u}}_{\mathbf{m}} = 0 \tag{4}$$

where ρ is the mass density and $\omega = 2\pi f$ the circular frequency. Equation (4) is the well-known Lamé-Navier equation for harmonic regimen. Displacement $\mathbf{u}$ associated by (3) to any complex amplitude $\hat{\mathbf{u}}_{\mathrm{m}}$ that is solution of this equation, can be discomposed in longitudinal $\mathbf{u}_{\mathrm{L}}$ and transversal $\mathbf{u}_{\mathrm{T}}$ components, that propagate respectively with phase velocities

$$c_{\mathrm{L}} = \sqrt{\frac{\lambda_{\mathrm{L}} + 2\mu_{\mathrm{L}}}{\rho}} \tag{5}$$

$$c_{\mathrm{T}} = \sqrt{\frac{\mu_{\mathrm{L}}}{\rho}} \tag{6}$$

2.2 Guided waves in plates and the 2D Helmholtz scalar equation

Wave propagation in plates is usually analyzed in terms of particular combinations (called modes) of longitudinal and transversal displacement characterized by transversal stationary displacement distributions.[12] For a given temporal frequency, each mode travels with a characteristic phase velocity along a direction contained in plane (x_1, x_2). In the most common case of plates with stress-free boundaries, modes can be classified into two groups: the so called horizontal shear (SH) modes that have displacement vectors $\mathbf{u}_{\mathrm{SH}}$ parallel to plane (x_1, x_2) and the Lamb modes, with displacement vectors $\mathbf{u}_{\mathrm{SV}}$ that have in-plane and out-of-plane components (see figure 1) and characterized by the frequency spectrum represetend in figure 2.

SH modes can be described in terms of one scalar potential, but Lamb modes are usually described by using scalar and vector potentials simultaneously (see f.i. reference 12). Recently, an alternative has been developed by Achenbach and coworkers that describe Lamb modes with only one scalar potential ϕ and two one-dimensional

functions $W_n(x_3)$ and $V_n(x_3)$ that characterize transversal shapes for the mode labeled n.[13] The out-of-plane component is simply given by $u_{n,3} = W_n(x_3)\,\phi(x_1, x_2)$. Hence, as the scalar potential $\phi(x_1, x_2)$ verifies the two-dimensional scalar Helmholtz equation in plane (x_1, x_2), it is evident that for each mode n, the equation

$$\Delta \hat{u}_{n,3m} + k_n^2 \hat{u}_{n,3m} = 0 \tag{7}$$

is also verified for any plane $x_3 = constant$ within the plate. Δ denotes the two-dimensional laplacian operator in (x_1, x_2) and k_n the Lamb wavenumber.

2.3 Scattering of guided waves in plates by through-thickness defects

At this point we will restrict the scope of the analysis to scattering phenomena generated by defects with two-dimensional geometry (as the case of a through-thickness hole with residual depth $e = 0$, see figure 1). In these conditions plate geometry is two-dimensional, in the sense that it depends only on (x_1, x_2) coordinates. When scattering is produced in conditions in which only one propagating Lamb mode contributes to u_3, then equation (7) can be employed. Following the approach of reference 11 we will assume that this is the case.

Then, if Γ denotes the boundary of the two-dimensional through-thickness defect and $\hat{u}_{3m}$ denotes complex amplitude associated to the out-of-plane component $u_3(x_1, x_2, h)$ of the scattered field, we can model our problem by means of the Partial Differential Equation

$$\begin{cases} \Delta \hat{u}_{3m} + k^2 \hat{u}_{3m} = 0 \quad \text{outside} \quad \Gamma \\ \frac{\partial \hat{u}_{3m}}{\partial n}|_\Gamma = g, \end{cases} \tag{8}$$

where g is a function defined on Γ. Stress-free conditions at defect boundary imply conditions on the spatial derivatives of the scattered field as a function of the spatial derivatives of the incident field. For this reason a generic Neumann Boundary condition is stated.

The validity of this model can be justified a posteriori on the basis of the comparison of model results with experimental data. Nevertheless, and although it is not the objective of this paper to justify model (8) and its conditions of applicability from fundamental equations of linear elasticity (1)-(4) we provide a brief a priori justification of our assumption for the case of through-thickness defects. This can be done by referring to an analytical model based on Achenbach approach for describing the scattering of Lamb waves by cylindrical holes in plates.[14] In this reference it is kept clear that an exact description of the scattering process requires SH modes for taking into account modal conversion effects at the cylinder border. Also, SH and Lamb evanescent modes have to be included in order to fulfill the stress-free boundary conditions. Nevertheless, for defects with two-dimensional geometry modal conversion occurs only between in-plane components. This means that u_3 displacements for Lamb modes, are not mixed with contributions of SH modes. Also, a few wavelengths away from the defect, contributions of the evanescent modes are not relevant. Hence, the out-of-plane component can be described as a superposition of incident and scattered Lamb modes. When only one propagating Lamb mode contributes to the out-of-plane component, Helmholtz equation is completely justified. The same is true when several contributions from Lamb modes exist, but all with the same frequency and Lamb wavenumber. This is the case of Rayleigh waves, that can be understood in the context of guided waves in plates as a superposition of S0 and A0 modes in their overlapping zone of the spectrum (see figure 2).

3. MATERIALS AND METHODS

3.1 Test plates

Experiments were performed in aluminium plates with dimensions 300 mm × 100 mm × 10 mm and with through-thickness holes and slots adequatelly prepared. The longitudinal wave velocity was measured by means of the classical pulse-echo method, resulting $c_L = 6358$ m/s.

Areas without defects were employed for analizing the incident field. Boundary conditions were studied employing the edge of the plates. In all cases plates were supported so that the constraints at their surface are minimized; they simply rest on a horizontal board covered in velvet fabric. Plasticine was used as acoustic absorber at the edges of the plates to avoid reflections of the incident and scattered waves that could disturb the measured acoustic fields (figure 3).

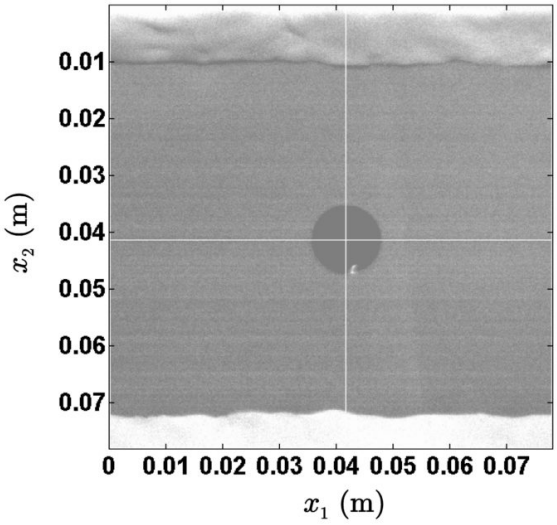

Figure 3. Reference image for a through-thickness hole ($e = 0$) of $D = 12$ mm.

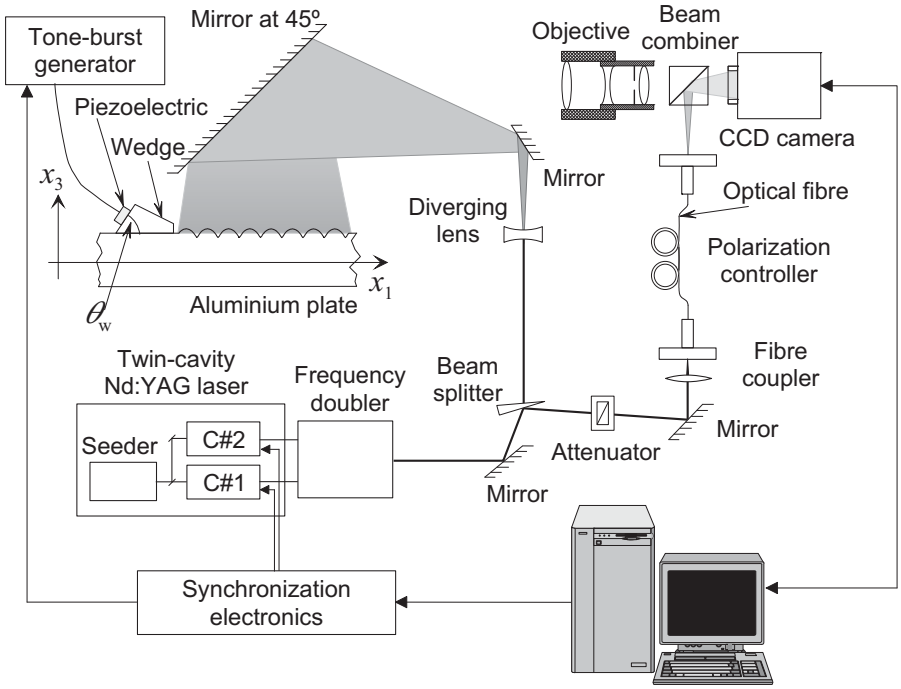

Figure 4. Experimental set-up.

3.2 Description of the experimental system

The lay-out of the experimental system used to generate and to detect the elastic waves is depicted in figure 4.

For this set of experiments a central temporal frequency of $f = 1.000$ MHz was employed. Rayleigh waves were generated by means of the classical wedge method, in which the longitudinal wave emitted by a piezoelectric transducer is coupled to the plate surface through a Bakelite prismatic coupling block of angle $\theta_{\mathrm{w}} = 65°$ (Fig. 4). A long tone-burst consisting of 99 cycles with a central frequency $f = 1.000$ MHz was used to excite the piezoelectric, in a way that the generated Rayleigh wavetrains are quasi-monochromatic.

Under these circumstances, the stress at the plate surface caused by the wedge presents a periodicity given by λ_1 and moves at a velocity c_{p} that correspond, respectively, to the wavelength λ_{R} and the phase velocity c_{R} of the Rayleigh wave at the frequency f. The wavelength of the produced quasi-monochromatic Rayleigh wave λ_{R} was measured with the procedure described in reference 15, resulting $\lambda_{\mathrm{R}} = 2.96$ mm, so that the Rayleigh phase velocity is given by $c_{\mathrm{R}} = \lambda_{\mathrm{R}} f$, resulting $c_{\mathrm{R}} = 2930$ m/s.

On the other hand, the instantaneous out-of-plane acoustic field $u_3(\mathbf{r}, t)$ at the plate surface due to the propagation of the Rayleigh wavetrain is measured with a self-developed double-pulsed TV holography system,[4] which has been successfully employed to measure quasi-monochromatic guided waves in plates with non-specular finish. The core of the system is a twin-cavity pulsed, injection seeded and frequency doubled Nd:YAG laser (Spectron SL404T), which emits two laser pulses with a duration of 20 ns that are used as the illumination source. Then, two correlograms are recorded in separate frames of a CCD camera (PCO Sensicam Double-Shutter). Each correlogram corresponds to the interference of a reference beam and an object beam scattered back by the plate surface. The system is set up to be sensitive to the out-of-plane component of the displacement of the surface points. For maximizing sensitivity, the delay of the laser pulses is set to 3 half-periods of the Rayleigh wave (i.e., the minimum number of odd half-periods for which the camera can record the two correlograms in different frames).

A processing procedure based on the spatial Fourier transform method is applied to the correlograms,[16] which renders the so-called optical phase-change map $\Delta\Phi(\mathbf{r}, t)$, proportional to the instantaneous out-of-plane acoustic displacement field $u_3(\mathbf{r}, t)$, i.e.:

$$\Delta\Phi(\mathbf{r}, t) = \frac{8\pi}{\lambda} u_3(\mathbf{r}, t) \tag{9}$$

being λ the wavelength of the laser and t the instant of emission of the first laser pulse.

3.3 Procedure for obtaining the experimental complex amplitude

The optical phase-change map given by (9) represents itself a useful means to assess the interaction of the Rayleigh wave and the defect. However, a second processing procedure based on the Fourier transform can be applied in order to improve signal-to-noise ratio and to calculate the acoustic amplitude $u_{3\mathrm{m}}(\mathbf{r}, t) = \mathrm{mod}\left[\hat{u}_{3\mathrm{m}}(\mathbf{r}, t)\right]$ and the total acoustic phase $\varphi_{3\mathrm{T}}(\mathbf{r}, t) = \arg\left[\hat{u}_{3\mathrm{m}}(\mathbf{r}, t)\right]$ of the Rayleigh wave, from which the complex amplitude

$$\hat{u}_{3\mathrm{m}}(\mathbf{r}) = u_{3\mathrm{m}}(\mathbf{r}) \exp\left(\varphi_{\mathrm{m}}(\mathbf{r})\right) \tag{10}$$

of the ultrasonic field can be obtained by simply selecting and arbitrary value of time t_0 for which $\varphi_{\mathrm{m}}(\mathbf{r}) = \varphi_{\mathrm{m}}(\mathbf{r}, t_0)$. Our procedure[17] consist of an improved version of previous method described in reference ,[16] that is based on the spatio-temporal 3D Fourier transform of a set of optical phase-change maps corresponding to successive instants delayed by a quarter of the wave period. In our case, eight optical phase-change maps delayed 250 ns were taken in each experiment and the spatio-temporal 3D Fourier transform method was applied to the whole set. The obtained experimental complex amplitude is the raw data for the comparison with numerical simulations.

3.4 Numerical Method

In order to efficiently produce accurate solutions of problem (8), we utilize a modified version of a highly efficient and accurate numerical methodology introduced recently,[18] which we describe briefly in what follows.

As it is well known, the (unique) solution of the Neumann Problem (8) can be expressed as a double-layer potential

$$\hat{u}_{3\mathrm{m}}(\mathbf{r}) = \int_{\Gamma} \frac{\partial G_k(\mathbf{r}, \mathbf{r}')}{\partial \mathbf{n}'_{\mathbf{r}}} \mu(\mathbf{r}') d\ell' \Gamma. \tag{11}$$

Here G_k denotes the Hankel function

$$G_k(\mathbf{r}, \mathbf{r}') = \frac{i}{4} H_0^1(k|\mathbf{r} - \mathbf{r}'|) \tag{12}$$

and, letting N denote the hypersingular operator

$$N(\mu)(\mathbf{r}) \equiv \lim_{z \to 0} \frac{\partial}{\partial \mathbf{n}_{\mathbf{r}}} \int_{\Gamma} \frac{\partial G_k(\mathbf{r}, \mathbf{r}' + z\mathbf{n}_{\mathbf{r}'})}{\partial \mathbf{n}'_{\mathbf{r}}} \mu(\mathbf{r}') d\ell', \tag{13}$$

the density μ is the unique solution of the first kind integral equation

$$N(\mu) = g. \tag{14}$$

Once the unknown surface density μ has been obtained, the solution $\hat{u}_{3\mathrm{m}}$ of equation (8) can be produced at any point outside Γ by applying numerical quadrature to equation (11).

Our numerical solver produces approximate solutions μ of equation (14) for a given right-hand side g by seeking a set of values $\mu_j \approx \mu(\mathbf{r}_j)$ of the unknown μ at a set of points $\mathbf{r}_j$ $(j = 1, \ldots, n)$ on the curve Γ. The algorithm relies on a highly accurate approximation of the integral equation (14) which can be obtained by appealing to an expression of the right-hand side of equation (13) that only uses tangential derivatives, in conjunction with interpolation of the values μ_j by trigonometric polynomials and exact differentiation and integration of trigonometric monomials. In order to resolve high curvatures while taking advantage of the excellent properties of trigonometric interpolation, the method utilizes smooth changes of variables that map an equi-spaced grid in the interval $[0, 2\pi]$ to a grid on Γ that contains a high density of discretization points $\mathbf{r}_j$ in high curvature portions of Γ. Note, in particular, that as a result of this discretization strategy, the density of discretization points $\mathbf{r}_j$ varies smoothly along Γ. The method then proceeds by constructing a linear system of equations for the quantities μ_j, which arises as the discretized version of the left-hand-side in equation (14) is set to equal the right hand side of that equation at each point $\mathbf{r}_j$, $j = 1, \ldots, n$. The algorithm is then completed by solving this linear system by means of a numerical implementation of the Gaussian elimination method. It was verified through a variety of numerical experiments, including comparisons with exact solutions, that the solutions $\hat{u}_{3m}$ produced by this methodology are highly accurate, and that the associated errors decay rapidly as discretizations are refined.

4. RESULTS AND DISCUSSION

4.1 Incident field characterization

In order to know the characteristics of the incident acoustic field and the repeatability of the measured maps, a series of acquisitions in the same conditions was performed within time intervals of 5 minutes. After processing the raw images in the same manner with identical parameters, the deviations between maps were of the order of 20 percent for both amplitude and real part (figure 5). Taking into account that the typical value of the amplitude was about 5 nm, these values are in accordance with a previous estimation of the noise of the technique.[3] Other features of interest are the slight curvature of the wavefronts and a non-uniform amplitude profile in a section transversal to the main propagation direction that complicates the comparison with numerical results.

4.2 Boundary conditions

To gain understanding about the boundary conditions to apply at the border of the defects, we studied the reflection of the incident acoustic field at the straight edge of a plate without defects for different incidence angles. The obtained results (Fig. 6) show that boundary conditions do not depend substantially on the incidence angle and also that, although the observed BC are neither Dirichlet nor Neumann, they are not far from the Neumann ones. So, we adopted them as a starting point for the numerical simulations of the scattering patterns.

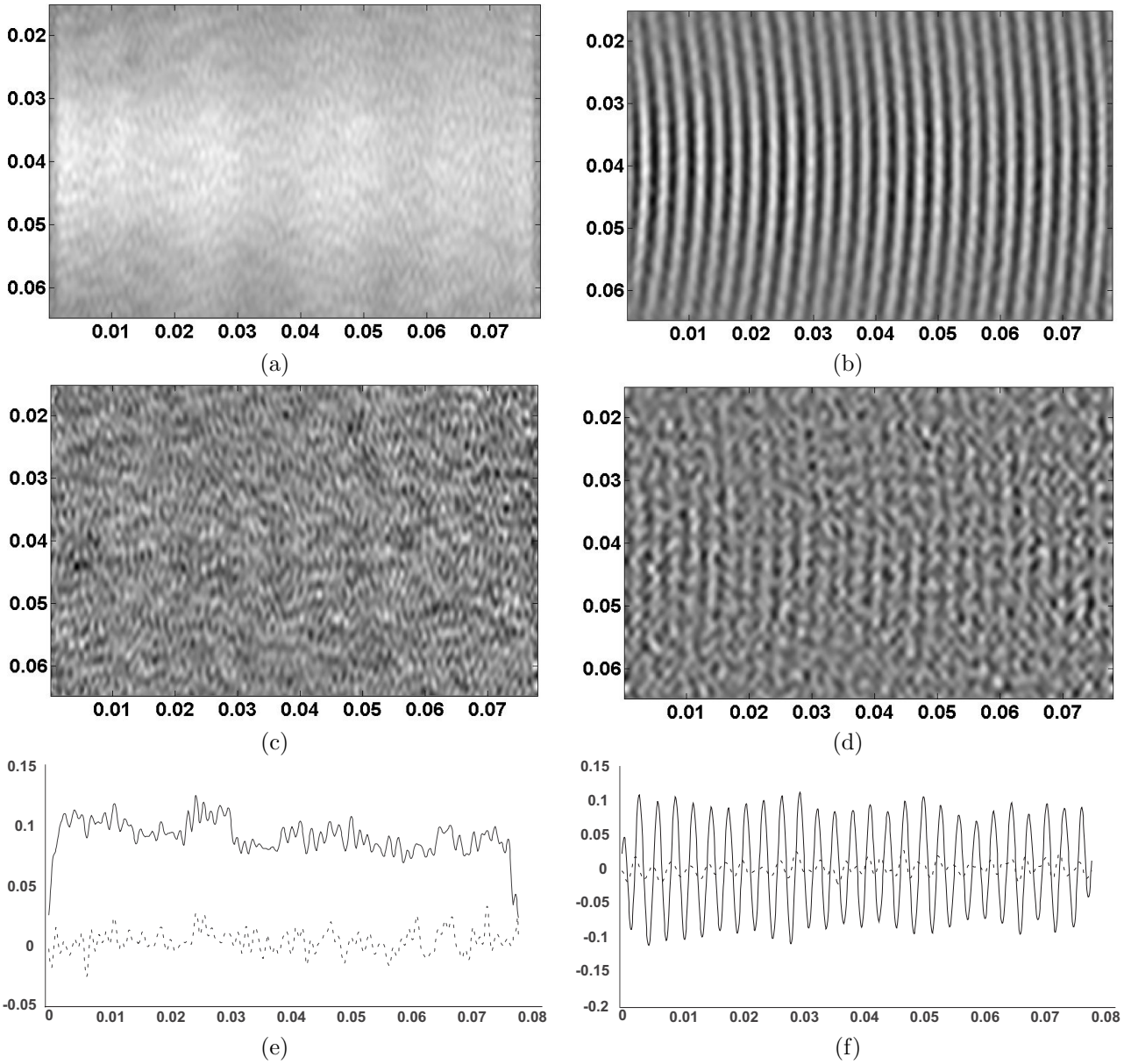

Figure 5. Repeatibility results. a) modulus of reference incident field, b) real part of a), c) difference of the modulus of reference field and another equivalent incident field, d) difference of the real parts of reference field and another equivalent incident field, e) horizontal profiles of a) (solid) and c) (dashed), f) horizontal profiles of b) (solid) and d) (dashed). Dimensions in meters. Mid-grey level represents zero. Profile amplitude in units of $\lambda/4\pi$. The axis numbering in a),b),c) and d) corresponds to that of figure 3

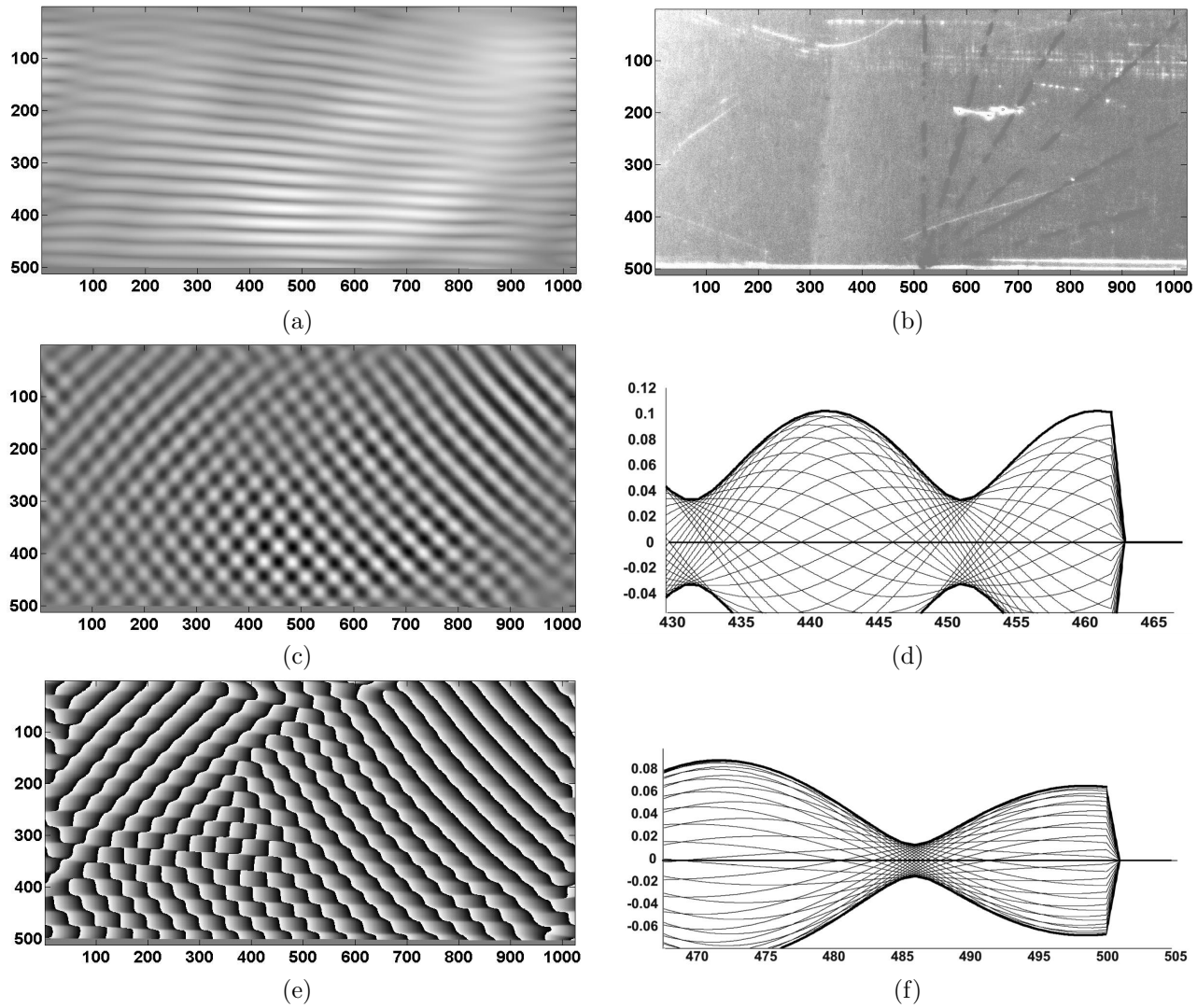

Figure 6. Results for the boundary conditions at the edge of the plate. a), c) and e) modulus, real part, and phase of the complex amplitude of the total field respectively, b) reference image of the plate and the edge, d) and f) profiles of the real parts for several time delays (thin) with the modulus envelope (thick). a), b), c), d) and e) correspond to incident angle of 45°, f) the same as d) but for 0° incidence angle. Dimensions in pixels. Profile amplitude in units of $\lambda/4\pi$. Mid-grey level represents zero. The axis numbering of a), b), c) and e) corresponds to that of figure 3

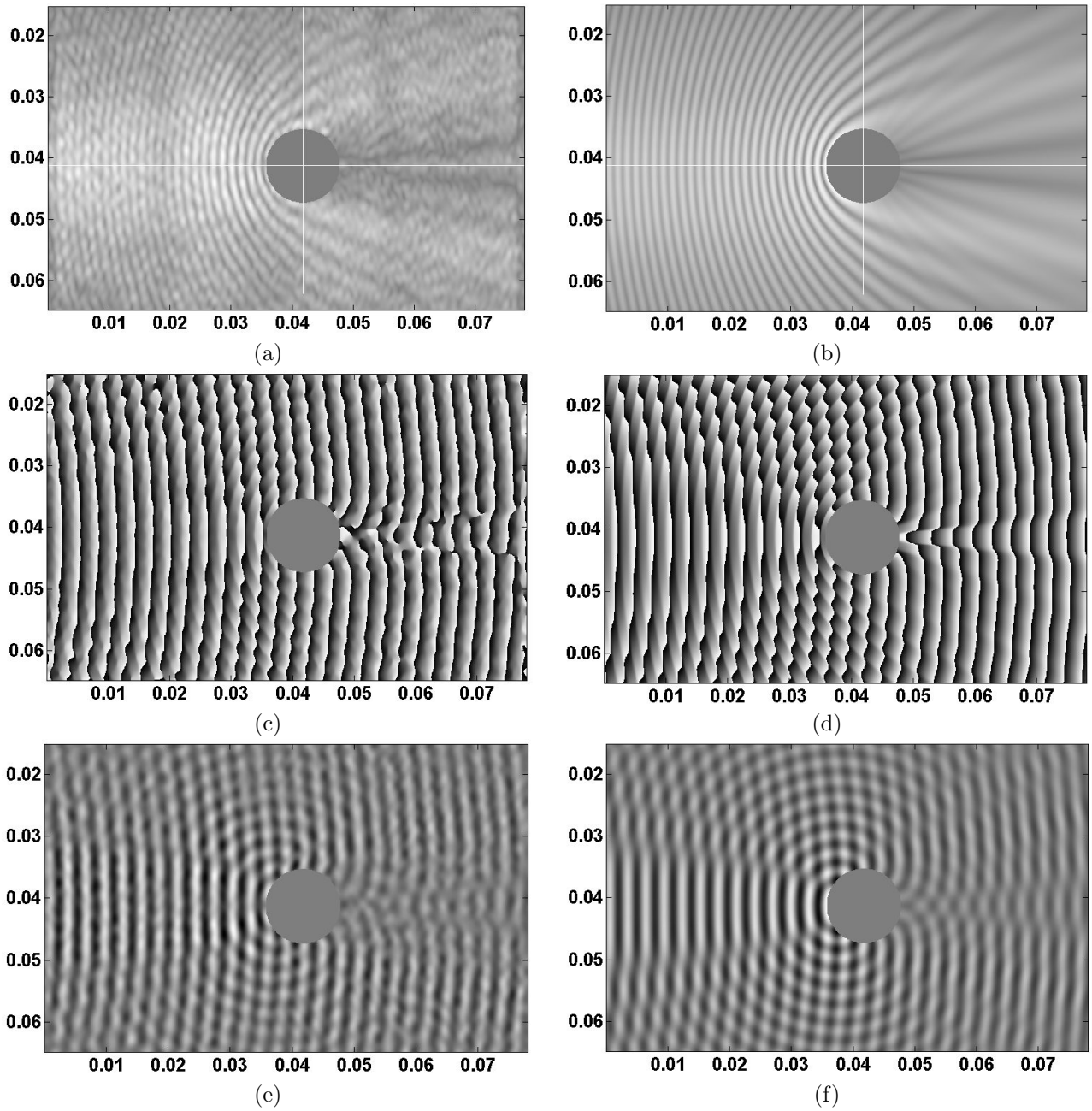

Figure 7. Scattering patterns for a cylindrical hole with D= 12 mm: comparison of complex amplitudes, a)-c)-e) experimental, b)-d)-f) numerical; a)-b) modulus, c)-d) phase, e)-f) real part. Dimension in meters. Mid-grey level represents zero. The axis numbering corresponds to that of figure 3

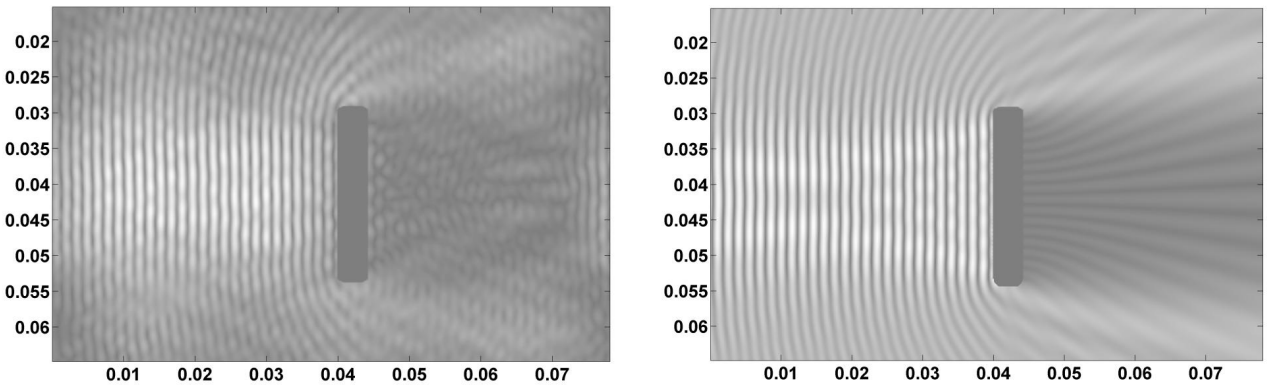

(a) (b)

Figure 8. Scattering patterns for a slot of mean width 24 mm. Modulus of complex amplitude: a) experimental b) numerical. Dimension in meters. Mid-grey level represents zero. The axis numbering corresponds to that of figure 3

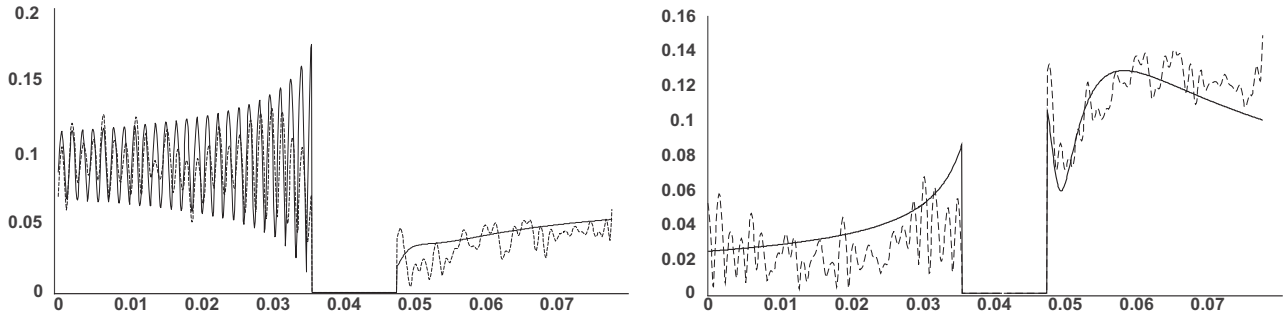

(a) (b)

Figure 9. Profiles for complex amplitud corresponding to hole of diameter D=12mm.: a) modulus of complex amplitude of the total field, b) modulus of complex amplitude of scattered field; amplitude in units of $\lambda/4\pi$; (dashed) experimental, (solid) numerical, Profiles along white horizontal line marked in figure 3

4.3 Scattering patterns

In figures 7 and 8 the comparison between the experimental and simulated scattering patterns of Rayleigh waves corresponding to two holes and a slot are presented. A simple visual inspection reveals their close agreement in the three cases in modulus, phase and real part. A quantitative analysis was performed by comparing the profiles along a central line of the maps, both for the total and scattered fields (Fig. 9). Even the main features of scattering pattern appear well correlated, pixel-to-pixel agreement between maps is not as good as their 2D visual matching. This is in consonance with measured noise levels. At this point, image processing techniques that average or reject the noise on the basis of spatial or morphological filtering could be applied. In any case, we believe that the presented results are enough to say that the experimental contrast of the numerical simulation is positive.

5. CONCLUSIONS

Scattering of elastic waves in plates has been studied employing two-dimensional maps of instantaneous out-of-plane displacements obtained with a self-developed pulsed TV-holography system. Experimental data have been compared with simulated scattering pattern employing an state of the art numerical technique. The achieved agreement gives support to the employed two-dimensional model. To improve the reliability of this model, further work should be done to analyze more defect typologies and sizes under different Lamb modes and frequencies.

ACKNOWLEDGMENTS

This work was co-funded by the Spanish *Ministerio de Ciencia e Innovación* and by the European Comission (ERDF) in the context of the *Plan Nacional de I+D+i* (project number DPI2008-02709) and by the *Dirección Xeral de Investigación, Desenvolvemento e Innovación da Xunta de Galicia* in the context of the *Plan Galego de IDIT* (project number INCITE08PXIB303252PR). Supplementary co-funding from the *Universidade de Vigo* (project number I608122F64102) is also acknowledged. Faisal Amlani and Oscar Bruno gratefully acknowledge support by the Air Force Office of Scientific Research and the National Science Foundation.

REFERENCES

[1] Birks, A. S., [*Nondestructive Testing Handbook*], vol. 7, American Society for nondestructive testing, Cambridge (1990).

[2] Bond, L., "Numerical techniques and their use to study wave propagation and scattering - a review," in [*Elastic waves and ultrasonic nondestructive evaluation*], S.K. Datta, J.D. Achenbach, Y. R., ed., 17–27, Elsevier Science Publisher (1990).

[3] Fernández, J. L., Doval, A. F., Trillo, C., Deán, J. L., and López, J. C., "Video ultrasonics by pulsed TV holography: A new capability for non-destructive testing of shell structures," *International Journal of Optomechatronics* **1**(2), 122–153 (2007).

[4] Trillo, C., Cernadas, D., Doval, A. F., López, C., Dorrío, B. V., and Fernández, J. L., "Detection of transient surface acoustic waves of nanometric amplitude with double-pulsed TV holography," *Applied Optics* **42**(7), 1228–1235 (2003).

[5] Cho, Y. and Rose, J., "A boundary element solution for a mode conversion study on the edge reflection of lamb waves," *J. Acoust. Soc. Am.* **99**(4), 2097–2109 (1996).

[6] Morvan, B., Wilkie-Cahncellier, N., Duflo, H., Tinel, A., and Duclos, J., "Lamb wave reflection at the free edge of a plate," *J. Acoust. Soc. Am.* **113**(3), 1417–1425 (2003).

[7] Castaings, M., Clezio, E. L., and Hosten, B., "Modal decomposition method for modeling the interaction of lamb waves with cracks," *J. Acoustic. Soc. Am.* **112**, 2567–2582 (2002).

[8] Masserey, B. and Mazza, E., "Analysis of the near-field ultrasonic scattering at a surface crack," *J. Acoustic. Soc. Am.* **118**, 3585–3594 (2005).

[9] Liu, G., "A combined finite element/strip method for analysing elastic wave scattering by cracks and inclusion in laminates," *Computational Mechanics* **28**, 76–81 (2002).

[10] Wang, C. and Chang, F.-K., "Scattering of plate waves by a cylindrical inhomogeneity," *Journal of Sound and Vibration* **282**(), 429–451 (2005).

[11] Mast, T. and Gordon, G., "Quantitative flaw reconstruction from ultrasonic surface wavefields measured by electronic speckle pattern interferometry," *IEEE Transactions on Ultrasonics, Ferroelectrics, and Frequency Control* **48**(2), 432–444 (2001).

[12] Rose, J. L., [*Ultrasonic Waves in Elastic Media*], 200–240, Cambridge University Press, Cambridge (2000).

[13] Achenbach, J. D., [*Reciporcity in elastodynamics*], 116–131, Cambridge University Press, Cambridge (2003).

[14] Dilligent, O., Grahn, T., Bostrom, A., Ccawley, P., and M.J.S.Lowe, "The low-frequecy reflection and scattering of the s0 lamb mode from a circular through-thickness hole in a plate: Finite element, analytical and experimental studies," *J. Acoust. Soc. Am.* **112**(6), 2589–2601 (2002).

[15] Deán, J. L., Trillo, C., Doval, A. F., and Fernández, J. L., "Determination of thickness and elastic constants of aluminum plates from full-field wavelength measurements of single-mode narrowband Lamb waves," *Journal of the Acoustical Society of America* **124**(3), 1477–1489 (2008).

[16] Trillo, C., Doval, A. F., Cernadas, D., López, O., López, J. C., Dorrío, B. V., Fernández, J. L., and Pérez-Amor, M., "Measurement of the complex amplitude of transient surface acoustic waves using double-pulsed TV holography and a two-stage spatial Fourier transform method," *Measurement Science & Technology* **14**(12), 2127–2134 (2003).

[17] Trillo, C. and Doval, A. F., "Spatiotemporal Fourier transform method for the measurement of narrowband ultrasonic surface acoustic waves with TV holography," *Proceedings of SPIE* **6341**, 63410B (2006).

[18] Bruno, O. P. and Lintner, S. K., "Generalized Calderon formula and second-kind integral solvers for TE and TM problems of diffraction by open arcs," *In Preparation* , (2009).